Proceedings of the ASME 2010 3rd Joint US-European Fluids Engineering Summer Meeting and 8th International Conference on Nanochannels, Microchannels, and Minichannels
FEDSM-ICNMM2010
August 1-5, 2010, Montreal, Canada

FEDSM-ICNMM2010-30570

LARGE-EDDY SIMULATION ON THE EFFECT OF AMBIENT PERTURBATION ON VEHICLE AERODYNAMICS

Makoto Tsubokura
Hokkaido University
Sapporo-shi, Hokkaido, Japan

Yuki Ikawa
Hokkaido University
Sapporo-shi, Hokkaido, Japan

Masashi Kitayama
Fuji Heavy Industries Ltd.
Ota-shi, Gunma, Japan

Takuji Nakashima
Hiroshima University
Higashi Hiroshima-shi, Hiroshima, Japan

ABSTRACT

A large eddy simulation method based on a fully unstructured finite volume method was developed, and the unsteady aerodynamic response of a road vehicle subjected to transient crosswinds was investigated. The method was first validated on the 1/20-scale wind tunnel model at a static aerodynamic condition and showed good agreement in the surface pressure distributions. The method was then applied to two transient crosswind situations: a sinusoidal perturbation representing the typical length scale of atmospheric turbulence, and a stepwise crosswind velocity corresponding to a wind gust. Typical transient responses of the aerodynamic forces and moments such as phase shifting and undershoot or overshoot were observed, and their dependence on the frequency and amplitude of the input perturbation is discussed. As a result, the utility and validity of LES is demonstrated in the context that such transient aerodynamic forces are difficult to measure in the conventional wind tunnel measurements.

INTRODUCTION

In the automotive industry, the aerodynamic performance of road vehicles has been principally evaluated through the aerodynamic coefficients such as C_D, C_L or C_M, which have been utilized for the improvement of fuel consumption or the estimation of vehicle maneuverability, and so on. In that context, these aerodynamic coefficients have been obtained in a static condition, in which a target vehicle is mounted on the floor of a wind tunnel with inlet flows that are uniform and smooth. However, considering that the real atmospheric wind to which a vehicle is subjected during on-road driving is fully turbulent (e.g., Cooper and Watkins in 2007), it is reasonable to suggest that discrepancies of the aerodynamic coefficients could appear between the cases of fully static and turbulent flows. The possible handling of the continuous relative yaw-angle change of the vehicle against the incoming flow by surrounding wind fluctuation would count the dependence of the aerodynamic coefficients on the yaw angle under the quasi-steady assumption (Cooper and Campbell, 1983). Thus, the aerodynamic coefficients have been ordinarily measured by rotating a vehicle over a range of yaw angles in a wind tunnel. The problem of the quasi-steady assumption is that it only treats relatively low-frequency responses, and hence it is impossible to consider the effects of a dominant turbulence mode. Concerning the turbulence mode, Cogotti (2003) developed and installed the Turbulence Generation System (TGS) in a full-scale wind tunnel and measured the drag and lift under an ambient turbulence condition (Cogotti, 2004). It has been reported that the mean C_D and front C_L increase compared with the case without ambient turbulence.

In addition to C_D, C_L or C_M for the estimation of fuel consumption and maneuverability, C_S and C_N are indispensable for estimating and achieving the safety in a gusty crosswind condition. The conventional method of assessing the crosswind safety is also based on the quasi-steady analysis using the averaged aerodynamic coefficients as a function of the yaw angle measured in a wind tunnel. However, the limitation of the quasi-steady analysis was pointed out by Beauvais (1967), who demonstrated that C_N seriously overshoots just after a vehicle is subjected to a wind gust and then decreases to steady-state. Dominy and Ryan (1999), from the same viewpoint, developed crosswind active shutters mounted on the side of the test section

of a wind tunnel and measured the transient surface pressure distributions.

Even though many research activities concerning the unsteady aerodynamic response caused by ambient turbulence and wind gusts have been recently conducted using innovative experimental setups, the knowledge acquired is limited due to the difficulty of capturing the unsteady aerodynamic forces and restricted physical values to be measured. In addition, additional experimental setups for the unsteady aerodynamics cost too much and are not suitable for the development process.

Computational Fluid Dynamics (CFD) is an attractive approach for the problem as it can provide a large amount of transient data and detailed three-dimensional information on the flow field (e.g., Okumura and Kuriyama, 1997; Guilmineau and Chometon, 2008; Hemida and Krajnović, 2009), which can help to elucidate the comprehensive mechanisms of the unsteady aerodynamics of road vehicles. However, the conventional Reynolds-averaged Navier-Stokes (RANS) simulation is only restrictive for the transient analysis, especially in the case when the fluctuating incoming flow interacts with the wake turbulence of the vehicle. In fact, even for the simplified vehicle called the Ahmed reference model (Ahmed and Ramm, 1984), the wake flow is fully unsteady and three-dimensional, together with the separation at the trailing edge of the roof and reattachment depending on the rear slant angle of the vehicle. The recirculation bubbles above the slant deck and their interaction with the wake vortices produce large elongated trailing vortices, causing a high induced drag. Reproduction of these complicated unsteady flows is indeed challenging for turbulence simulations, and only a limited success has been achieved so far by Reynolds-averaged Navier-Stokes (RANS) approaches (e.g., Guilmineau, 2008).

A promising candidate for that purpose is the Large-Eddy Simulation (LES), in which larger eddies are directly solved while smaller and universal eddies are only modeled. Thus, the physical mechanism of the transient aerodynamic response caused by the unsteady three-dimensional eddies is possibly explained through the method. Therefore, the objective of this study was to develop a numerical method based on LES and to study the transient aerodynamic response caused by ambient turbulence and wind gusts. Recently, some attempts have been made to apply LES to the Ahmed flow (e.g., Krajnović and Davisdon, 2005ab). Fares (2006) adopted the lattice Boltzmann method instead of the spatially filtered Navier-Stokes approach and demonstrated the validity of the unsteady flow simulation. Minguez et al. (2008) proposed a high-order LES based on a multi-domain spectral Chebyshev-Fourier approach. In this study, we will focus on the real production vehicle as a typical engineering application. The difficulty of the target lies in the fact that owing to the complicated geometry compared with the Ahmed model, only a limited numerical approach such as a fully unstructured finite volume/element or voxel mesh can be applied.

The ambient turbulence has been simplified to be a sinusoidal transversal velocity imposed on the main inlet, and, as a result, the relative yaw angle β with respect to the incoming flow has continuously changed. In the same way, the crosswind gust has been represented by the simple stepwise transversal velocity imposed on the main flow.

NOMENCLATURE

- A amplitude of the sinusoidal crosswind velocity [m]
- A_s frontal area of the vehicle [m^2]
- C_D drag coefficient (=$2F_x/\rho V_0^2 A_s$)
- C_L lift coefficient (=$2F_z/\rho V_0^2 A_s$)
- C_S side force coefficient (=$2F_y/\rho V_0^2 A_s$)
- C_M pitching moment coefficient (=$2M_y/\rho V_0^2 A_s L$)
- C_N yawing moment coefficient (=$2M_z/\rho V_0^2 A_s L$)
- f frequency of the crosswind [Hz]
- F_x drag force [N]
- F_y side force [N]
- F_z lift force [N]
- H height of the vehicle [m]
- L length of the vehicle [m]
- M_x roll moment [Nm]
- M_y pitch moment [Nm]
- M_z yaw moment [Nm]
- S_t Strauhal number (=fL/U_0)
- u_i velocity for i direction [m/s]
- U_0 main inlet velocity [m/s]
- v transversal (crosswind) velocity [m/s]
- V_0 relative velocity acting on the vehicle [m/s] (=$(U_0^2+v^2)^{1/2}$)
- W width of the vehicle [m]
- β angle of yaw [°]
- λ wave length of sinusoidal crosswind velocity [m]
- ν kinetic viscosity [m^2/s]
- ρ density of the incoming fluid [kg/m^3]

Subscripts and superscript

- x, y, z main streamwise, transversal, vertical
- $1, 2, 3$ main streamwise, transversal, vertical
- $+$ wall unit normalized by the kinetic viscosity and the surface friction

NUMERICAL METHODS

Governing Equations

An incompressible and Newtonian fluid was assumed, and the continuity and momentum equations were spatially filtered to obtain the governing equations of LES, which read as:

$$\frac{\partial \overline{u}_i}{\partial x_i} = 0 \quad , \tag{1}$$

$$\frac{\partial \overline{u}_i}{\partial t} + \frac{\partial \overline{u}_i \overline{u}_j}{\partial x_j} = -\frac{\partial \overline{P}}{\partial x_i} + 2\frac{\partial}{\partial x_j}(\nu + \nu_{sgs})\overline{S}_{ij} \quad , \tag{2}$$

in which u_i, ν and ρ are the velocity for the i direction, kinetic viscosity, and fluid density, respectively. The bar over the physical quantity indicates the spatial filtering operation for LES. The filtered strain rate tensor $\overline{S}_{ij}$ and pressure $\overline{P}$ in Eq. (2) are expressed as

$$\overline{S}_{ij} = \frac{1}{2}\left(\frac{\partial \overline{u}_j}{\partial x_i} + \frac{\partial \overline{u}_i}{\partial x_j}\right), \tag{3}$$

$$\overline{P} = \overline{p}/\rho + (\overline{u_i u_j} - \overline{u}_i \overline{u}_j)/3 . \tag{4}$$

In Eq. (2), the last term on the right represents the effect of subgrid-scale (SGS) turbulence, which is modeled under the eddy viscosity assumption. The conventional Smagorinsky's model (Smagorinsky, 1963) was adopted, and the eddy viscosity coefficient is modeled as

$$\nu_{sgs} = (C_s f_d \Delta)^2 \sqrt{2\overline{S}_{ij}\overline{S}_{ij}}, \tag{5}$$

in which C_s is the model coefficient determined prior to the simulation, Δ is the length scale of the SGS turbulence and is expressed as a cube root of each numerical mesh, and f_d represents the damping effect of SGS turbulence at the vicinity of the solid wall. The van Driest type damping function was adopted in the study, which is given as

$$f_d = 1 - \exp\frac{-l^+}{25}, \tag{6}$$

where l^+ is the distance from the solid wall in the wall coordinate normalized by the surface friction and the kinetic viscosity.

For the model parameter, Cs=0.1 was adopted in this study. The value was optimized on the surface pressure distribution of the vehicle in Fig. 1 among the three values of 0, 0.1 and 0.15. While the results were relatively sensitive to the value between Cs=0.1 and 0.15, the former showed better agreement with the experimental data, especially at the rear end region.

Discretization

The governing equations were discretized in space by a vertex-centered unstructured finite volume method. Second-order central differences were mainly applied for the spatial derivative, blended with the first-order upwind scheme for the convective term in the Navier-Stokes to avoid the excessive numerical oscillation appearing at coarse tetrahedral elements. It should be noted here that the dissipation property of upwind schemes is desirable to a certain extent for the engineering applications of LES on unstructured meshes. As a compromise, the contribution of the upwind discretization to the convective fluxes was set to be as low as 5%. The diffusive fluxes on the volume surface were treated based on the deferred correction formula suggested by Muzaferija (1994) to avoid the checkerboard-type oscillation. The MUSCL (Monotone Upwind Scheme for Conservation Law) scheme by van Leer (1977) was also adopted for the convective term at the region away from the vehicle where the upwind dissipation does not affect the wake and near-wall turbulence of the target vehicle.

The time marching was based on the fractional step method by Kim & Moin (1985), in which the third-order Adams-Moulton scheme or the implicit Euler scheme was adopted for the velocity prediction step. The coupling of the velocity and pressure fields to obtain the pressure and to correct the velocity was based on the SMAC (Simplified Marker and Cell) method by Amsden and Harlow (1970). The flow rate on the control-volume surface was estimated following the method proposed by Rhie and Chow (1983) to reduce the checkerboard-type pressure oscillation. The pressure Poisson equation was solved by the Incomplete Cholesky Conjugate Gradient (ICCG) method.

The computational code "Frontflow/red" adopted in the present study was originally developed under the "Frontier Simulation Software for Industrial Science" project in Japan. The code has been intensively optimized based on High-Performance Computing technique for LES of the vehicle aerodynamic (Tsubokura et al., 2007, 2008a, 2009).

Numerical Setups

The 1/20 wind tunnel model of a station-wagon-type vehicle is shown in Fig. 1. The definition of drag, side and lift forces, as well as pitch, roll and yaw moments with respect to each axis is also indicated. The overall length, width and height of the model are L=0.234 m, W=0.086 m, and H=0.074 m. The surface geometry of the vehicle body is precisely reproduced from the Computer-Aided Design (CAD) data of the real scale model, while its underbody is simplified to be flat and the engine room is omitted.

The solid surface is reproduced by triangular meshes with a

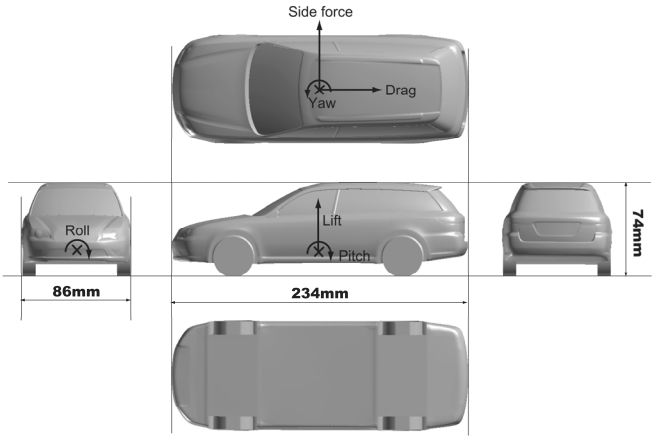

Fig. 1 The orthogonal views of the station-wagon vehicle (1/20th scale model).

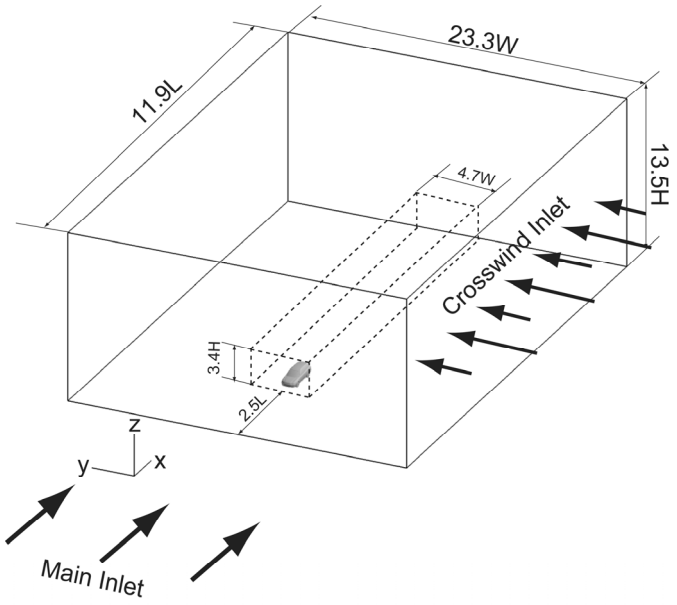

Fig. 2 Analysis region.

spatial resolution of a few mm and is covered by five layers of prism meshes to improve the accuracy of surface friction. The finest triangular meshes of less than 0.5 mm are allocated around the pillars and the trailing edge of the roof where fine turbulence eddies are generated, while relatively coarse meshes of around 1.2 mm are used under the vehicle and over the front window, where flow is attached on the wall. The minimum thickness of the nearest prism layer on the wall was determined so as to maintain its distance from the wall as less than 10 in wall unit l^+.

The rectangular computational domain, with its length, width, and height given as 11.9L, 23.3W, and 13.5H, is illustrated in Fig. 2. A uniform flow of U_0=18.5 m/s is the main inlet, and the vehicle is fixed on the floor at 2.5L downstream from the inlet plane. Another inlet condition is imposed on the side wall of the domain to reproduce continuous or gusty crosswind fluctuations. The same inlet velocity condition is given on the opposite side wall as a forced outlet condition to maintain a mass balance for the transverse direction. On the surface of the vehicle and the floor, the assumed profile for the main flow velocity (linear or log-law depending on the distance from the wall) is considered to determine the surface friction as a boundary condition on the wall. The free-slip velocity condition is given on the ceiling, and the gradient-free condition is imposed on the outlet plane. The outlet plane was set far away from the vehicle to avoid the influence of the error generated by the gradient-free condition at the outlet. The MUSCL scheme is mainly used except for the rectangular sub-region illustrated by broken lines, in which the second-order central finite difference scheme is adopted. To avoid excessive numerical oscillation induced by the central finite difference, relatively fine tetrahedral elements are allocated at the region where the second-order central method is used, as presented in Fig. 3. The total element and node numbers required for the simulation were about 20 million and 4 million, respectively.

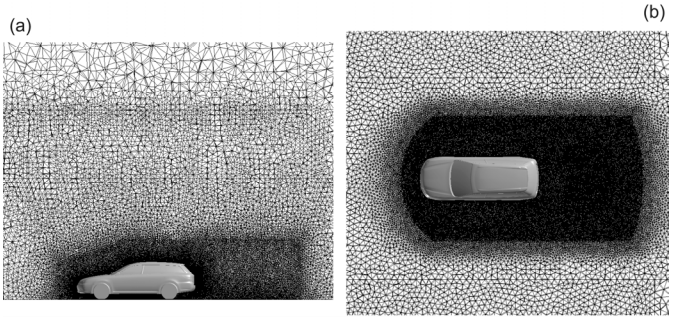

Fig. 3 Far-field grid allocations around the vehicle: (a) vertical section on the center-plane; (b) horizontal section on the floor.

In this study, the focus is a vehicle aimed straight ahead that is subjected to gusty or continuously fluctuating crosswinds. The flow field is reproduced in CFD by fixing the coordinate on the vehicle, and the fluctuating crosswind region is convected downstream at the same speed as the assumed vehicle velocity. To realize the convective crosswind, the lateral velocity profile of the crosswind is imposed on the side of the computational domain and is transported downstream at the same speed as the main inlet velocity (Tsubokura et al., 2008b). The corresponding wind-tunnel measurements were proposed and conducted by Dominy & Ryan (1999). The Reynolds number with respect to the main incoming flow U_0 and the vehicle length L amounts to 2.0×10^5.

All numerical simulations were conducted on an SR11000 (Hitach) supercomputer at the Information Technology Center, University of Tokyo. A total of eight nodes (128 CPUs) were used to calculate each time-step in 3.3 real seconds. The simulations were time-integrated by the Euler implicit method for the first six thousands steps with a time increment of $\Delta t=1 \times 10^{-5}$ to make the flow fully developed, and they were then switched by the Adams-Moulton method of $\Delta t=0.5 \times 10^{-5}$ for the next some ten thousands steps for the precise prediction of the unsteady aerodynamics. The time increment was determined so as to have the CFL number less than 2 and 1 for the Euler implicit and Adams-Moulton methods, respectively.

RESULTS AND DISCUSSIONS

Validation

The numerical method was validated in the static case in which the yaw angle β was fixed to 0°, 10°, 20°, and 30°, and the aerodynamic forces and moments acquired numerically were compared with the wind tunnel data obtained by Tanaka et al. (2006). It should be noted that the experimental data were measured at a wind tunnel with its test section fully opened. The diameters of the round open jet and the round rear collector

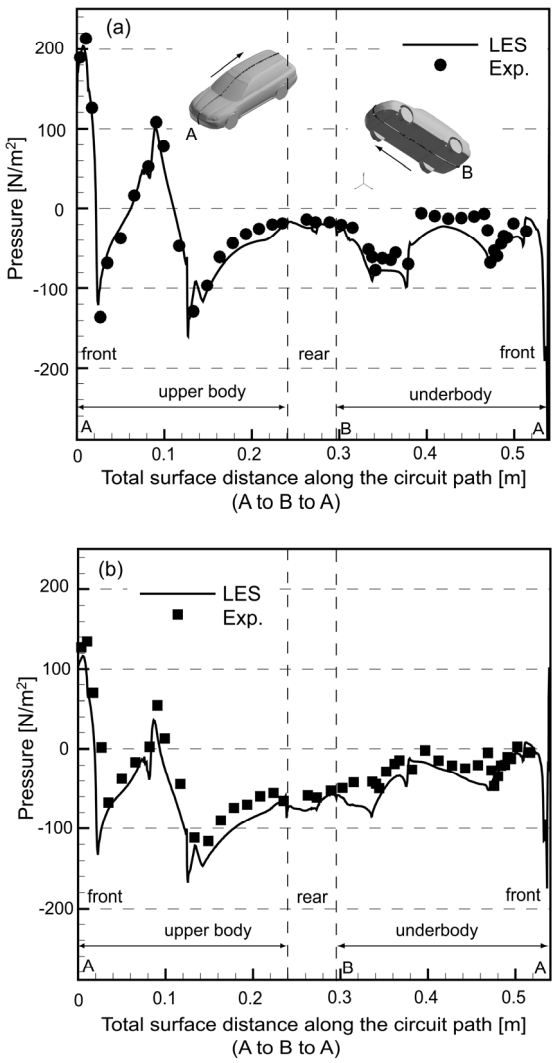

Fig. 4 Surface pressure distribution along the center-line in the static condition: (a) β=0 degrees; (b) β=30 degrees.

nozzles were 400 mm and 600 mm, respectively. The distance between these two nozzles was 720 mm, and the vehicle model was mounted on an acrylic plane with a length of 700 mm and a width of 800 mm. The vehicle centroid was located on the center-line and was 450 mm downstream from the front edge of the plane.

The surface pressure distributions on the center-line of the vehicle in the cases of β=0° and 30° are shown in Fig. 4. Generally, the LES results show good agreement with the experimental data. However, relatively large discrepancies are identified on the roof and rear end under the body in the case of β=30° as well as at the middle of the underbody in the case of β=0°. The possible explanation of the discrepancy is due to the difference of the test section geometry between the present LES and the experiment. In the LES, the test section was fully closed with a blockage ratio less than 0.4%, whereas that of the wind tunnel measurement was open with the open jet diameter at only 400 mm. Considering the fact that the length of the model is 234 mm, the interaction between the vehicle wake and the free shear layer of the jet is not ignorable as the yaw angle of the vehicle increases.

Continuous Yawing Change

To investigate the effect of unsteady ambient wind on the vehicle aerodynamics, and especially its aerodynamic response to some specific wind frequencies, sinusoidal transverse velocity profiles were overlapped on the main incoming flow. The crosswind profiles were imposed as an inlet/outlet boundary condition on both sides of the computational domain, as shown in Fig. 2, which is expressed as:

$$v = A\sin 2\pi(x/\lambda - ft) \quad . \quad (7)$$

Because the sinusoidal profile travels at the same velocity as the inlet velocity, the frequency is given by $f=U_0/\lambda$.

According to the on-road measurement conducted by Wordley and Saunders (2008), the integral length-scale of turbulence around a vehicle in on-road driving is strongly dependent on the ambient environment around the road. The maximum length has been observed in a smooth terrain and reaches up to around 20 meters, with a turbulence intensity as low as 2% to 6%. The minimum length has been identified in a freeway traffic condition and is less than five meters, while its turbulence intensity has a wide range up to 16%. In this study, two length-scales of about the same as (1.3L) and about three times (2.6L) the vehicle length were mainly considered. With the incoming velocity of 18.5 m/s, the frequency and the wavelength of the transversal velocity fluctuation imposed were set to f=60 Hz, λ=0.308 m (=1.3L) and f=30 Hz, λ=0.617 m (=2.6L). The corresponding Strouhal numbers (S_t) of the frequency with respect to L and U_0 are 0.76 and 0.38, respectively. For reference, a relatively longer length-scale of f=10 Hz, λ=1.85 m (=7.9L) corresponding to S_t=0.13 was also conducted.

The snapshots of the lateral velocity distributions around the vehicle and the surface pressure contour in the case λ=1.3L and β=±10° are visualized in Fig. 5. It is observed that the vehicle goes straight ahead through the sinusoidal crosswind. The crosswind is slightly decayed at the downstream of the vehicle, owing to the coarser numerical grids allocated. It is remarkable that, because the wavelength λ=1.3L is comparable to the vehicle length, the crosswind velocity with the opposite direction acts on the vehicle at the same time and multiple flow structures appear around the vehicle. The amplitudes of the fluctuation were determined so as to vary the relative yawing angle β of the vehicle with respect to the incoming flow between -10 and +10 or -15 and +15 degrees.

The time series of the aerodynamic forces and moments in the cases of β=±10°/λ=1.3L are plotted in Fig. 6. The crosswind

profiles measured at the horizontal centroid of the vehicle at 6.8H above the ground are also indicated. The sinusoidal aerodynamic responses of the side force as well as the yaw and

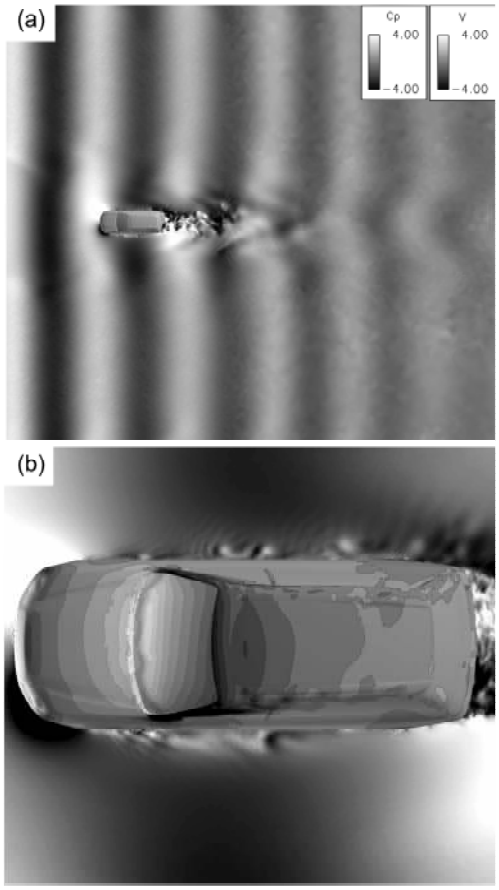

Fig. 5 Crosswind distribution around the vehicle and the surface pressure distribution: λ=1.3L and β=±10°.

roll moments are remarkable, while their phases are slightly shifted with respect to the crosswind velocity. The drag, lift, and roll also show sinusoidal responses with frequencies twice higher than the crosswind velocity, but they are contaminated by a still higher frequency mode.

The trajectories of the phase-averaged drag, side force, lift and yaw moment are illustrated in Fig. 7, in which the horizontal axis indicates the sinusoidal yawing as the input and the vertical axis represents the aerodynamic response as the output. The static aerodynamic forces measured by fixing the yaw angle at 0°, 10° and 20° at the corresponding relative incoming velocity V_0 against the vehicle are also plotted for reference. At this relatively smaller yawing change, all three indicated aerodynamic components increase almost linearly with respect to the yaw angle in the static case, as given by the dash-dotted line. The gradient lines are utilized for the analysis based on the quasi-steady assumption.

The drag and lift trajectory in all cases shows more or less a butterfly pattern, which suggests that the drag response has a

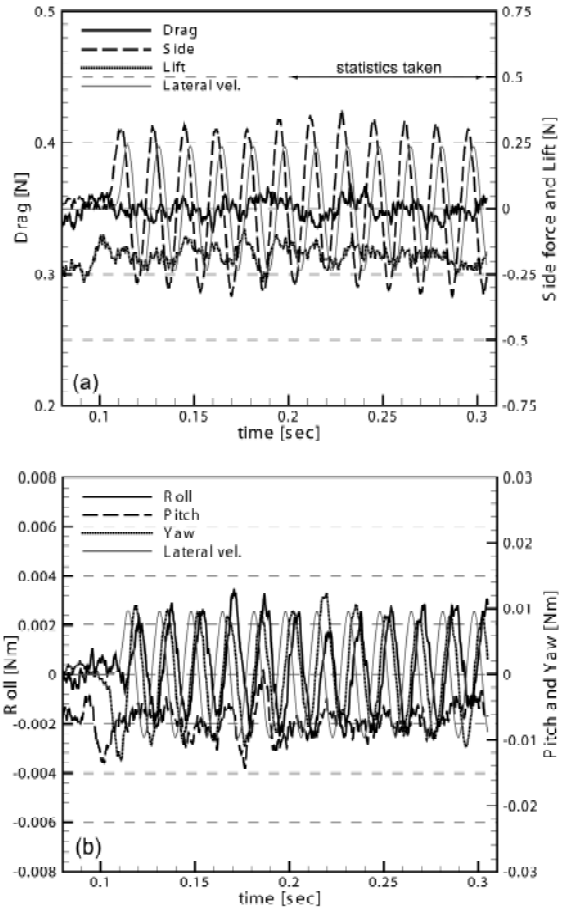

Fig. 6 Time history of unsteady aerodynamic forces and moments in a continuous yawing angle change; λ=1.3L and β=±10°: (a) Forces; (b) Moments.

frequency two times higher than that of the input sinusoidal yawing. As the wavelength becomes smaller, its dependence on the yaw angle represented by the gradient of the trajectory becomes smaller. In the drag trajectory, as a typical case of β=±15° and λ=2.6L, while its dependence on the continuous yawing is drastic, its displacement between β=-15° to 15° is ΔF_x~0.1 N, which is about the half of the value estimated from the quasi-steady assumption. In fact, the dependence on the continuous yawing represented by the gradient of the trajectory is less than the quasi-steady line. On the other hand, in the case of the smaller wavelength of λ=1.3L, significant dependence on the continuous yawing disappears. With regard to the mean drag under continuous yawing, it slightly increases at the wavelength of λ=2.6L, as shown in Table 1. As the wavelength become smaller and more comparable to the vehicle length, no significant increases of the averaged drag are identified.

The trajectory of the side force and yaw moment is ellipsoidal and rotationally symmetric, representing that the aerodynamic response is sinusoidal with a frequency that is the same as the sinusoidal yawing. The width of the ellipsoid

reflects the phase shift with respect to the continuous yawing frequency. In both cases, the elliptical trajectory at the same wavelength of λ=2.6L is similar between β=10° and 15°,

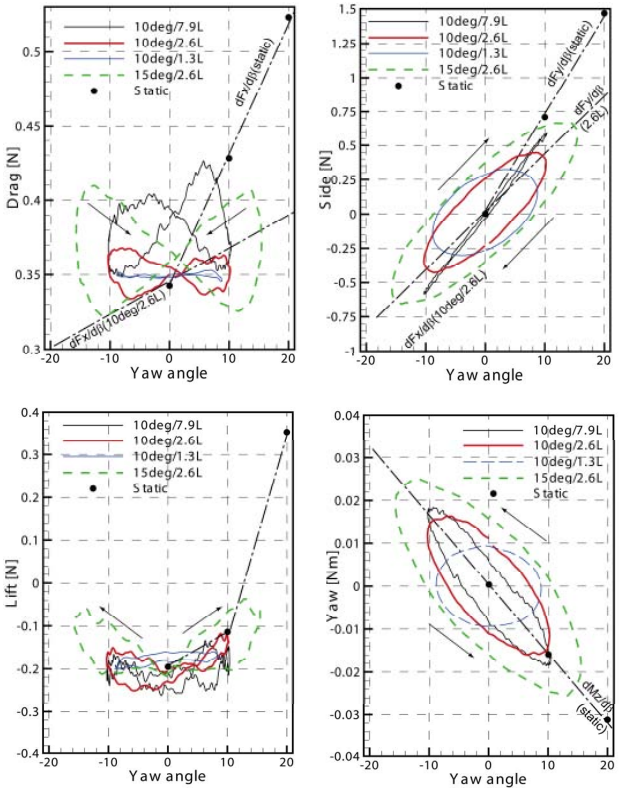

Fig. 7 Trajectory of the aerodynamic response: upper left, drag force; upper left, side force; lower left, lift; lower right, yaw moment.

indicating that they are synchronized with each other and that the only difference is the magnitude, which strictly follows the relative velocity V_0.

In the side-force trajectory, as the wavelength λ increases to 7.9L, it becomes almost linear and is close to the quasi-steady line; hence, no significant unsteady effect is observed. On the other hand, as the wavelength λ becomes smaller and more comparable to the vehicle length, the trajectory becomes more circular, which suggests that the phase shift against the input yawing becomes larger. It is interesting to note that the gradient of the side force $dF_y/d\beta$ at λ=2.6L against the yaw angle represented by the major axis of the ellipse and expressed by the dash-dotted lines in the figure, is less steep compared with the static case (quasi-steady). As the wavelength is reduced to half, $dF_y/d\beta$ slightly decreases. Accordingly, the discrepancy of the side force between the dynamic case at the maximum yaw amplitude and the static case becomes wider as the yaw angle increases or the wavelength decreases. Generally speaking, the unsteady effects such as the phase sift or the difference from the quasi-steady assumption appear when the wavelength is more than three times the vehicle length.

On the other hand, in the yaw moment, the phase shift represented by the elliptical trajectory appears even at λ=7.9L and is enhanced as the wavelength becomes smaller, while the gradient of the yaw moment $dM_z/d\beta$ is identical between the static and the dynamic case at λ=2.6L and 7.9L. In addition, contrary to the side force, the yaw moments at the maximum yaw amplitude of β=10° in the case of β=±10°/λ=2.6L, 7.9L and in the static case are also almost identical. In the same manner, the maximum magnitude of the yaw moment at β=±15° in the case of β=±15°/λ=2.6L can be estimated by the quasi-steady prediction. The dependence of $dM_z/d\beta$ on the wavelength between λ=2.6L and 1.3L is also notable. It is significantly declined at λ=1.3L, and its major axis is close to being horizontal, suggesting that the averaged moment at the specific yaw angle is less dependent on the yaw angle at the wavelength comparable to the vehicle length. With regard to the mean lift force and the mean pitch moment, they are more or less affected by the sinusoidal yawing, as shown in Table 1. The lift is strongly affected by the imposed magnitude A and that the downforce is almost 35% decreased by the continuous yawing change at β=15°. The pitch, on the other hand, depends on the frequency imposed, and its magnitude is 20% decreased when increasing the wavelength from λ=1.3L to λ=2.6L.

Table 1 Averaged drag, lift and pitch moments in the continuous yawing case

	Steady flow	β=±10° λ=2.6L	β=±10° λ=1.3L	β=±15° λ=2.6L
Drag [N]	0.343	0.348	0.348	0.364
Lift [N]	-0.195	-0.189	-0.182	-0.127
Pitch [Nm] $\times 10^{-3}$	-7.56	-6.05	-6.89	-6.06

Gusty Crosswind

To understand the influence of an unexpected gust on the aerodynamic performance of the vehicle, a stepwise transversal velocity profile was imposed on the main incoming flow. The crosswind profile was determined to realize the situation when the straight-ahead vehicle rushes into the crosswind region and the relative yaw angle of the vehicle with respect to the incoming flow rapidly changes from 0° to 30°. The velocity of the main incoming flow was fixed at U_0=18.5 m/s, and the transversal velocity changed from 0 to 10.7 m/s. The imposed crosswind is not exactly stepwise but was approximated by the 6th-order polynomials to avoid the numerical oscillation.

The time history of the acquired unsteady aerodynamic forces is illustrated in Fig. 8. The nose and tail of the vehicle reach the crosswind interface at T=0.283 s and 0.296 s, respectively, and the shaded area indicates that the vehicle has been subjected to the crosswind for this time period. Because the incoming flow velocity increases from 18.5 to 21.4 m/s during the process, all six aerodynamic forces finally increase to

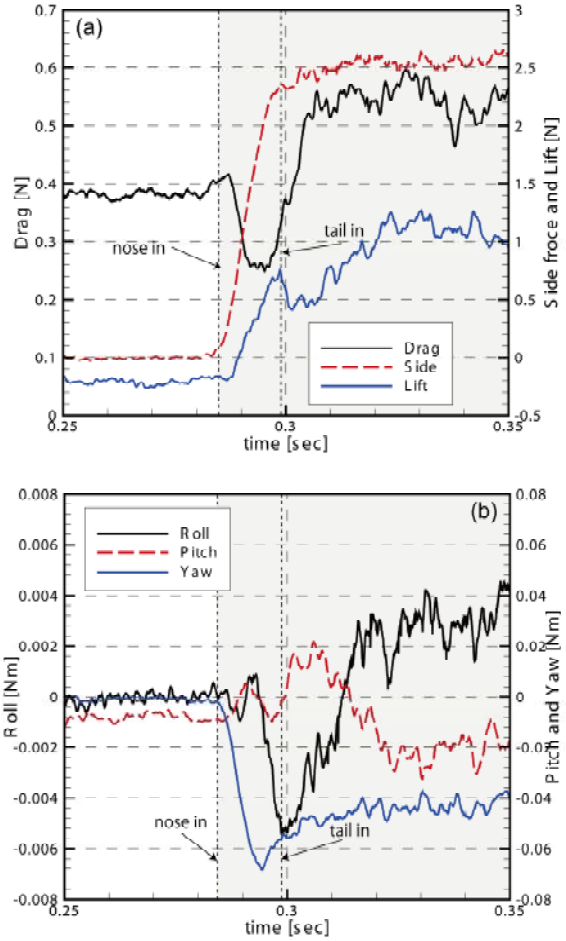

Fig. 8 Time history of unsteady aerodynamic forces and moments in a sudden crosswind: (a) Forces; (b) Moments.

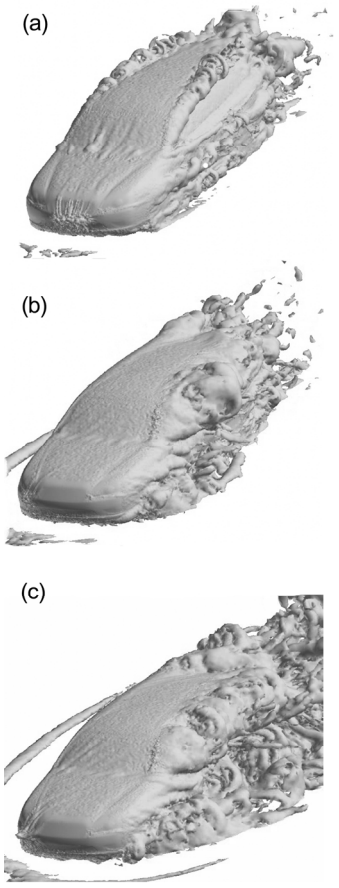

Fig. 9 Snapshots of the iso-surface of vorticity magnitude before, during, and after the rushing-in process: (a) T=0.25 s; (b) T=0.29 s; and (c) T=0.32 s.

some degree when a sufficiently long time passes after the rushing-in process. On the other hand, their transient growth is independent of the static yaw-angle case indicated in Fig. 7. While the side force increases monotonically against time, the drag undershoots and the lift overshoots just after the nose reaches the crosswind interface, and then monotonically increase to reach the steady-state. It is notable that compared with the drag and side forces, a relatively longer time period is required for the lift to reach a static state representing the fixed β=30° case.

The non-linear aerodynamic response with respect to the time path is more clearly observed in the moments, in which all three components show drastic overshoots or undershoots. Among them, the undershoot of the yaw moment has been widely acknowledged (e.g., Beauvais, 1967). It is also reported that this undershoot is caused by the separation at the corner of the vehicle and thus is geometry dependent. The sudden increases of the pitch moment and the lift force are also remarkable because they degrade the running stability of vehicle. In addition, similar to the lift force, these two components also show a relatively longer relaxation time for reaching the steady state. It seems that distances that are two to three times longer than the vehicle length are required for the aerodynamic response to be fixed down after the nose of the vehicle reaches the crosswind interface, and hence the transient response lasts until around t=0.33 s.

To investigate the non-linear response and the time delay, the flow structures and surface pressure are visualized. Figure 9 shows snapshots of vortical structures around the vehicle at three consecutive times before, during and after the rushing-in process. The typical flow structures, such as the front pillar or the front tire-house vortices, are identified just before the rush-in and are symmetric with respect to the vehicle center-plane. Intensive flow separation at the leeward front pillar is identified just after the rush-in, as shown in Fig.9(b), while the wake is seemingly not affected by the crosswind. The development of the side separation continues until it runs down to the wake and interacts with each other, as shown in Fig.9(c).

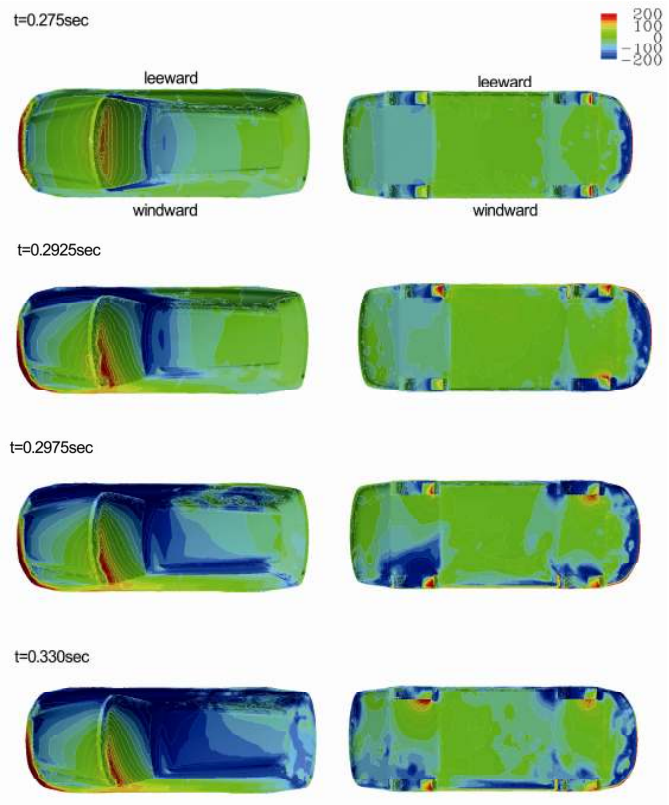

Fig. 10 Snapshots of the pressure contours on the vehicle surface at T=0.275, 0.2925, 0.2975, and 0.330 s.

The time variation of the surface pressure snapshot is visualized in Fig. 10. The separation of the flow at the windward corner of the roof represented by the low pressure is remarkable at T=0.2925 s and propagates downstream as time passes. At T=0.330 s, the separation can be observed at the entire windward corner of the roof. The propagation of the separation also enhances the separation above the roof, and the low-pressure region spreads over the roof. However, the process is rather sequential and does not explain the nonlinear increase of the lift, pitch and roll observed in Fig. 8. On the other hand, drastic unsteady phenomena can be observed under the body. At T=0.2975 s, just after the entire body is subjected to the crosswind, a flow separation represented by the low pressure is found behind the windward front and rear wheels, while the separation is mitigated as time passes, as shown at T=0.330 s. The undershooting of pitch and roll as well as the overshoot of the lift are observed at around T=0.2975 s; thus, it is reasonable to say that this is caused by the intensive flow separation around the windward side.

CONCLUSIONS

An LES method for the unsteady aerodynamics of road vehicles was developed based on a fully unstructured finite volume method, and the unsteady aerodynamic response of a road vehicle subjected to two types of transient crosswinds was investigated.

In the continuous sinusoidal yawing case, all six components of the aerodynamic forces and moments showed more or less sinusoidal responses, with phase shifts depending on the imposed wavelength. The unsteady effect represented by the difference from the quasi-steady assumption was remarkable when the wavelength was comparable to the vehicle length. Considering the fact that the typical integral length-scale of ambient wind around a road vehicle is comparable to the vehicle length (Wordley and Saunders, 2008), the limitation of the quasi-steady assumption based on conventional wind tunnel measurements was determined to take into account the ambient turbulence in vehicle aerodynamics.

In the gusty crosswind case, overshoot or undershoot of the transient aerodynamic forces and moments during the vehicle rushing into the crosswind region was demonstrated. In addition to the well-known undershoot of the yaw moment reported by Beauvais (1967), the drag, lift, pitch and roll also showed non-linear responses. The relaxation time to reach each aerodynamic force or moment at a statistically steady-state was found to depend on each component, and relatively longer time periods were required for the lift force as well as the roll and pitch moments. The reason for the longer relaxation time was explained by the transient reaction of underbody flow, which is represented by the drastic separation and mitigation observed around the windward wheels. This result reflects the importance of underbody shape for the crosswind safety.

ACKNOWLEDGMENTS

This work was mainly supported by the Industrial Technology Research Grant Program in 2007 from the New Energy and Industrial Technology Development Organization (NEDO) of Japan. It was partly supported by a Grant-in-Aid for Scientific Research from JSPS (No. 20560143) and the NRL of NRF of Korea (R0A-2008-000-20069-0). This study was conducted in a collaborative research project with Fuji Heavy Industries Ltd., and the shape data and experimental data received are greatly acknowledged.

REFERENCES

Ahmed, S. R., Ramm, G., and Galtin, G., 1984, “Some salient features of the time-averaged ground vehicle wake”, SAE Technical paper series, 840300

Amsden, A. A. and Harlow, F. H., 1970, “A simplified MAC technique for incompressible fluid flow calculations”, Journal of Computational Physics, vol. 6, pp.322-325

Beauvais, F. N., 1967, “Transient nature of wind gust effect on an automobile”, SAE Technical Paper 670608

Cooper, K. R., and Campbell, W. F., 1983, “An examination of the effects of wind turbulence on the

aerodynamic drag of vehicle", Journal of Wind Engineering and Industrial Aerodynamics, vol. 9, pp.167-180

Cooper, K. R., and Watkins, S., 2007, "The unsteady wind environment of road vehicles, Part one: A review of the on-road turbulent wind environment", SAE Technical Paper Series 2007-01-1236

Cogotti, 2003, "Generation of a controlled level of turbulence in the Pininfarina wind tunnel for the measurement of unsteady aerodynamics and aeroacoustics", SAE Technical Paper Series 2003-01-0430

Cogotti, 2004, "Update on the Pininfarina "turbulence generation system" and its effects on the car aerodynamics and aeroacoustics", SAE Technical Paper Series 2004-01-0807

Dominy, R. G., and Ryan, A., 1999, "An improved wind tunnel configuration for the investigation of aerodynamic cross wind gust response", SAE Technical Paper Series 1999-01-0808

Fares, E., 2006, "Unsteady flow simulation of the Ahmed reference body using a lattice Boltzmann approach", Computers & Fluids, vol. 35, pp.940-950

Guilmineau, E., "Computational study of flow around a simplified car body", 2008, Journal of Wind Engineering and Industrial Aerodynamics, vol. 96, pp.1207-1217

Guilmineau, E., and Chometon, F., 2008, "Numerical and experimental analysis of unsteady separated flow behind an oscillating car model", SAE Technical Paper Series 2008-01-0738

Hemida, H. and Krajnović, S., 2009, "Transient simulation of the aerodynamic response of a double-deck bus in gusty winds", Journal of Fluids Engineering, Transactions of ASME, vol. 131, pp.031101-1~031101-10

Kim, J. and Moin, P., 1985, "Application of a fractional step method to incompressible Navier-Stokes equations", Journal of Computational Physics, vol. 59, pp.308-323

Krajnović, S. and Davidson, L., 2005, "Flow around a simplified car, Part 1: Large Eddy Simulation", Journal of Fluid Engineering, vol. 127, pp.907-918

Krajnović, S. and Davidson, L., 2005, "Flow around a simplified car, Part 2: Understanding the flow", Journal of Fluid Engineering, vol. 127, pp.919-928

van Leer, B., 1977, "Toward the ultimate conservative difference scheme 4, a new approach to numerical convection", Journal of Computational Physics, vol. 23, pp.276-99

Minguez, M., Pasquetti, R., and Serre, E., 2008, "High-order large-eddy simulation of flow over the "Ahmed body" car model", Physics of Fluids, vol. 20, 095101

Muzaferija, S., 1994, "Adaptive finite volume method for flow predictions using unstructured meshes and multigrid approach", Ph.D thesis, University of London

Okumura, K., and Kuriyama, T., 1997, "Transient aerodynamic simulation in crosswind and passing an automobile", SAE Technical Paper Series 970404

Rhie, C. M. and Chow W. L., 1983, "A numerical study of the turbulent flow past an isolated airfoil with trailing edge separation", AIAA Journal, vol. 21, pp.1525-32

Smagorinsky, J., 1963, "General circulation experiments with the primitive equations, I. The Basic Experiment", Monthly Weather Rev., vol.91, Num. 3, pp.99-164

Tanaka, F., Kawaguchi, K., Sunohara, K., Hasegawa, T., and Takada, K., 2006, "Flow around vehicle model (Study of numerical accuracy of yawing moment), Proc. of the 20th Symp. On Computational Fluid Dynamics, A6-2, in Japanese

Tsubokura, M., Kitoh, K., Oshima, N., Nakashima, T., Zhang, H., Onishi, K., and Kobayashi, T., 2007, "Large Eddy Simulation of unsteady flow around a formula car on Earth Simulator", SAE 2007 Trans. J. of Passenger Cars –Mechanical Systems, 2007-01-0106

Tsubokura, M., Kobayashi, T., Nakashima, T., Nouzawa, T., Nakamura, T., Zhang, H., Onishi, K. and Oshima, N., 2008a, "Computational visualization of unsteady flow around vehicles using High Performance Computing", Computers & Fluids, vol. 38, pp.981-990

Tsubokura, M., Nakashima, T., Ikenaga, T., Onishi, K., Kitoh, K., Oshima, N. and Kobayashi, T., 2008b, "HPC-LES for the prediction of unsteady aerodynamic forces on a vehicle in a gusty cross-flow condition, SAE Technical Paper 2008-01-300

Tsubokura, M., Nakashima, T., Kitoh, K., Sasaki, Y., Oshima, N., and Kobayashi, T., 2009, "Development of un unsteady aerodynamic simulator using large-eddy simulation based on high-performance computing technique", SAE Technical paper series 2009-01-0007

Wordley, S. and Saunders, J., 2008, "On-road Turbulence", SAE Technical Paper, No.2008-01-0475